

TESTING METHOD FOR INTERFACE MODE II FRACTURE OF PLAIN CONCRETE AND FIBER-REINFORCED CEMENTITIOUS COMPOSITE

**BO-TAO HUANG^{1,2}, XING YIN¹, QING-HUA LI^{1,*}, SHI-LANG XU¹,
YI-FENG ZHANG¹, YAO LYU¹, CHAO-JIE SUN¹, BO-KUN CHEN¹**

¹Institute of Advanced Engineering Structures and Materials, Zhejiang University
Hangzhou, China

e-mail: botaohuang@zju.edu.cn; yinxing@zju.edu.cn; liqinghua@zju.edu.cn (*corresponding author);
slxu@zju.edu.cn; zhangyf10@sunac.com.cn; lyuyao@zju.edu.cn; 11512037@zju.edu.cn;
chen_bk@zju.edu.cn

² Department of Civil and Environmental Engineering, The Hong Kong Polytechnic University
Hong Kong, China
e-mail: bthuang@polyu.edu.hk

Key words: Shear fracture; Interface; Testing method; Concrete; ECC; SHCC

Abstract: The performance of a bi-material interface is one of the major concerns in the repair or strengthening of concrete structural elements. In this study, a novel testing method for interface shear fractures of plain concrete and fiber-reinforced cementitious composites is proposed to avoid tensile failure during the test. Double-edge notched and unnotched specimens are utilized. Analytical, numerical, and experimental investigations are carried out to validate this method. The stress intensity factor K of the double-edge specimen with bi-materials is analytically obtained by the J -integral method. Based on ultra-high toughness cementitious composite (UHTCC)/concrete models, a numerical investigation of the proposed method is performed to confirm its suitability for shear fracture tests. Furthermore, the double-edge UHTCC/concrete specimens are experimentally investigated. The proposed method can be applied to obtain the interface shear parameters of concrete materials, which are needed for analytical or numerical analyses of bi-material interfaces in concrete structures.

1 INTRODUCTION

One common technique to repair or strengthen concrete structural elements is to add a new layer of concrete or cement-based materials to an existing concrete substrate, which is referred to as concrete jacketing. Among cement-based repair materials, the fiber-reinforced cementitious composite with a high ductility is considered one of the ideal materials to strengthen reinforced concrete structures [1, 2, 3, 4, 5]. This material is

developed based on the micromechanical principles proposed by Li and Leung [6]. Such

materials exhibit significant pseudo-strain-hardening responses and multi-cracking behaviors, and are referred to as engineered cementitious composites (ECCs) [7, 8], strain-hardening cementitious composites (SHCCs) [9, 10], or ultra-high toughness cementitious composites (UHTCCs) [11, 12]. Under both monotonic and fatigue loadings, a UHTCC has a significantly higher ductility than those of

conventional plain and fiber-reinforced concretes [13, 14, 15, 16, 17], and has potential applications to improve the mechanical performances and durability of concrete structures [1, 3, 5, 18, 19].

One of the major concerns in concrete jacketing is the performance of the bi-material interface. For UHTCC-based strengthening systems, the mechanical performance of the UHTCC/concrete elements is significantly affected by the interface delamination [1, 4, 5, 18]. For example, during bending of UHTCC-layered concrete beams, a shear stress concentration emerges once the concrete layer cracks [5, 18]; the shear stress then increases with the bending load. In numerous previous studies [5, 18, 20], interface delamination caused by the shear stress concentration was observed. The interface shear debonding may lead to reductions in the loading and deformation capacities of the strengthened elements [18]. For reliable applications of cement-based strengthening materials, it is of significance to investigate the shear fracture behavior of the interface.

Several schematic representations of interface shear fracture tests for concrete materials were summarized by Espeche and León [21]. As mentioned in [21], many of these interface shear tests induce bending moment forces, as they are far from generation of a theoretically pure shear state and the tensile stress cannot be avoided. For the interface between concrete materials, the tensile strength is low, which might lead to tensile failure prior to shear failure in these tests. Therefore, the development of a more suitable shear fracture testing method for concrete interfaces is essential. In addition, it is important to determine the interface shear properties, required for reliable analytical or numerical analyses of bi-material interfaces in strengthened concrete structures.

For identical concrete materials, a double-edge notched compression test was proposed by Reinhardt et al. [22, 23, 24] to achieve the pure shear (mode II fracture) testing, which has been numerically and experimentally validated. Inspired by this method, we proposed a novel testing method of interface

shear fractures of concrete materials. It provides a new approach to evaluate the interface shear fracture behaviors of concrete materials. In the following sections, a brief introduction of the double-edge notched specimen of identical materials is presented. A theoretical analysis is then performed to obtain the expressions of stress intensity factors of the proposed specimens. A numerical analysis is carried out to investigate the detailed stress distributions. Finally, an experiment is carried out to validate that the proposed method can be applied for the interface shear fracture tests of UHTCC/concrete specimens.

2 DOUBLE-EDGE SPECIMENS OF IDENTICAL MATERIALS

For the double-edge notched infinite plate, the ligament length is $2a$, while the in-plane tensile loading is σ . The Tada's elastic solution [25] is:

$$\begin{cases} K_I = 0 \\ K_{II} = \frac{1}{4} \sigma \sqrt{\pi a} \end{cases} \quad (1)$$

It should be noted that the mode I component is zero in this case. Additionally, if the x -directional total length is larger than $4a$ and the y -directional total depth is larger than $2\pi a$, the Tada's solution can be used [22, 23, 24].

For the double-edge notched infinite strip, the following solution was proposed by Xu et al. [26]:

$$\begin{cases} K_I = 0 \\ K_{II} = \frac{1}{4} \sigma \sqrt{\omega} \end{cases} \quad (2)$$

The mode I component is also zero. It is worth noting that if the x -directional total length is larger than $4a$ and the y -directional total depth 2ω is smaller than $2\pi a$, the Xu's solution can be used [22, 23, 24].

In the above cases, the condition that the x -directional total length is larger than $4a$ ensures a uniform distribution of stress at the loaded end of the strip. If there were other means to guarantee the uniform stress distribution, this condition could be relaxed [23, 24]. On the basis of the infinite strip, the

double-edge notched and unnotched specimens were proposed for shear fracture tests of concrete, as shown in Fig. 1. It has been numerically and experimentally confirmed that the double-edge notched specimen is suitable to carry out the pure shear test [22, 23, 24, 27]. A notable discontinuity point was observed in the load–displacement curve in the test. This point could be considered the critical shear fracture point. The double-edge unnotched specimen was systematically investigated by Gao [27]. For the unnotched specimen, a shear fracture also occurred; Eq. (2) can be used to calculate the stress intensity factor.

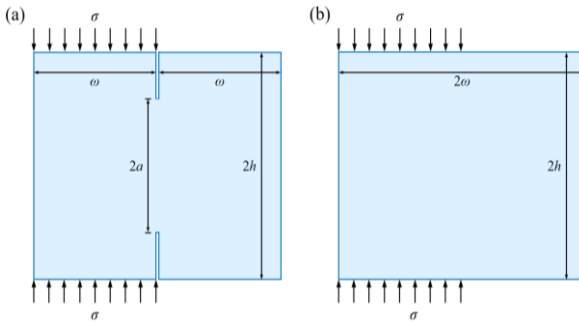


Fig. 1 Double-edge specimens (a) with and (b) without notches for shear fracture tests of concrete materials

3 DOUBLE-EDGE SPECIMENS OF BI-MATERIALS FOR INTERFACE SHEAR FRACTURE TESTS

The double-edge compression test, illustrated in Fig. 1, inspired us to propose a novel method for evaluation of the interface shear fractures of concrete materials. The double-edge specimens consisting of two materials (each edge corresponds to one material) are introduced to evaluate the interface shear fracture behavior, as shown in Fig. 2 (a). For concrete materials, the tensile strength is significantly lower than the compressive strength. Therefore, in the proposed method, the compression test is used for the double-edge specimen. With the increase in the compressive loading, the shear stress at the crack tip of the bi-material interface increases and an interface shear fracture is expected to appear. As mentioned in Section 2, the condition $h \geq 2a$ can be relaxed in a double-edge notched compression test if there were other methods to guarantee a

uniform stress distribution [22, 23, 24]. Therefore, the bi-material specimen without notches in Fig. 2 (b) can be also used when the uniform stress distribution is achieved.

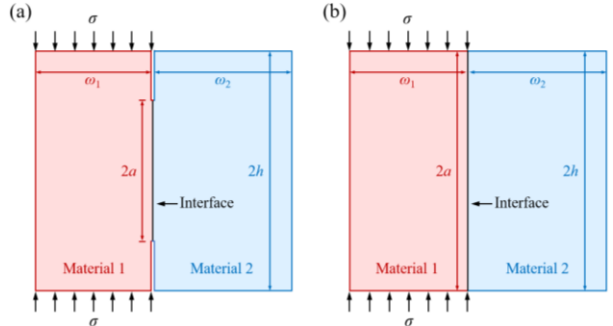


Fig. 2 Double-edge specimens (a) with and (b) without notches for interface shear fracture tests

The stress intensity factor K of the double-edge notched specimen with bi-materials in Fig. 2 (a) can be obtained by the J -integral method proposed by Rice [28]. Fig. 3 presents half of the specimen in Fig. 2; a linear distribution of the deformation along the symmetry axis of the specimen is assumed. Therefore, the deformation along the symmetry axis can be equivalent to a combination of an axial deformation ε and rotational deformation φ . The stress corresponding to ε and φ can be then determined at both layers and the stress distribution can be obtained. The equilibrium equations of the force and moment of the half specimen in Fig. 3 are Eqs. (3) and (4), respectively. The expressions of ε and φ can be obtained by solving the following two equations:

$$\begin{aligned} \sum N = 0 &\Rightarrow \\ \sigma\omega_1 &= \varepsilon(E_1\omega_1 + E_2\omega_2) \\ &+ \frac{1}{2}\varphi(E_1\omega_1^2 - E_2\omega_2^2) \end{aligned} \quad (3)$$

$$\begin{aligned} \sum M = 0 &\Rightarrow \\ \frac{1}{2}\sigma\omega_1^2 &= \frac{1}{2}\varepsilon(E_1\omega_1^2 - E_2\omega_2^2) \\ &+ \frac{1}{3}\varphi(E_1\omega_1^3 + E_2\omega_2^3) \end{aligned} \quad (4)$$

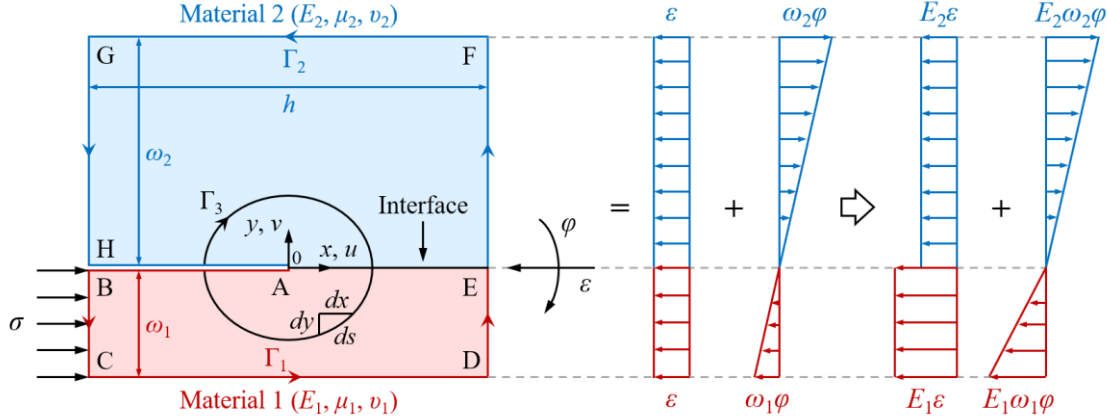


Fig. 3 Integral path and stress distribution of the double-edge notched specimen with bi-materials

The J -integral of the half specimen in Fig. 3 with identical materials has been reported in [29]. For the bi-material case in Fig. 3, the corresponding J -integral can be expressed in the following form:

$$\begin{aligned} J &= J_{\Gamma_1} + J_{\Gamma_2} \\ &= \int_{\Gamma_1} (\tau_{xy} du + \sigma_y dv - W_1 dy) \\ &\quad + \int_{\Gamma_2} (\tau_{xy} du + \sigma_y dv - W_2 dy) \end{aligned} \quad (5)$$

where W_i is the strain energy density:

$$\begin{aligned} W_i &= \frac{1}{2E_i} (\sigma_x^2 + \sigma_y^2 - 2\nu_i \sigma_x \sigma_y \\ &\quad + 2(1+\nu_i) \tau_{xy}) \quad (i=1, 2) \end{aligned} \quad (6)$$

where E_i , μ_i , and ν_i are the elastic moduli, shear moduli, and Poisson's ratios of the materials in Fig. 3, respectively.

The J -integral is path-independent. Therefore, the following integral path is chosen:

$$\begin{aligned} J &= \int_{AB} \dots + \int_{BC} \dots + \int_{CD} \dots + \int_{DE} \dots \\ &\quad + \int_{EF} \dots + \int_{FG} \dots + \int_{GH} \dots + \int_{HA} \dots \end{aligned} \quad (7)$$

The J -integral can be then obtained:

$$J = - \left(\int_{BC} W_1 dy + \int_{DE} W_1 dy + \int_{EF} W_2 dy \right) \quad (8)$$

where

$$W_i = \frac{\sigma_x^2}{2E_i} \quad (\tau_{xy} = 0, \sigma_y = 0, i=1, 2) \quad (9)$$

$$\begin{cases} \sigma_{x-\overline{BC}} = \sigma \\ \sigma_{x-\overline{DE}} = E_1 \varphi y - E_1 \varepsilon \\ \sigma_{x-\overline{EF}} = E_2 \varphi y - E_2 \varepsilon \end{cases} \quad (10)$$

Using Eqs. (9) and (10) in Eq. (8), the following expression of the J -integral can be derived:

$$\begin{aligned} J &= - \left(\int_0^{-\omega_1} \frac{\sigma^2}{2E_1} dy \right. \\ &\quad \left. + \int_{-\omega_1}^0 \frac{(E_1 \varphi y - E_1 \varepsilon)^2}{2E_1} dy \right. \\ &\quad \left. + \int_0^{\omega_2} \frac{(E_2 \varphi y - E_2 \varepsilon)^2}{2E_2} dy \right) \end{aligned} \quad (11)$$

The J -integral can be set equal to the linear elastic energy release rate G [28, 30]:

$$J = G \quad (12)$$

The energy release rate G of an interface crack between different elastic materials under a plane stress has been reported in [30, 31, 32, 33]:

$$G = \frac{1/E_1 + 1/E_2}{2 \cosh^2(\pi\alpha)} K^2 \quad (K^2 = K_I^2 + K_{II}^2) \quad (13)$$

where

$$\alpha = \frac{1}{2\pi} \ln \frac{\kappa_1/\mu_1 + 1/\mu_2}{\kappa_2/\mu_2 + 1/\mu_1} \quad (14)$$

$$\kappa_i = (3 - \nu_i) / (1 + \nu_i) \quad (i=1, 2) \quad (15)$$

$$\mu_i = \frac{E_i}{2(1+\nu_i)} \quad (i=1, 2) \quad (16)$$

$$K = \cosh(\pi\alpha) \sqrt{-\frac{2E_1E_2}{E_1+E_2} \left(\int_0^{-\omega_1} \frac{\sigma^2}{2E_1} dy + \int_{-\omega_1}^0 \frac{(E_1\varphi y - E_1\varepsilon)^2}{2E_1} dy + \int_0^{\omega_2} \frac{(E_2\varphi y - E_2\varepsilon)^2}{2E_2} dy \right)} \quad (17)$$

The expression of K can be obtained by introducing ε and φ into Eq. (17). However, the obtained final expression of K for the common cases is still complex. In the practical application of this testing method, the widths of the two materials (i.e., ω_1 and ω_2 in Fig. 2) can be adjusted to obtain a significantly simpler expression of K . According to Eqs. (3) and (4), simplified expressions of K can be obtained if the widths of the two edges and elastic moduli of the two materials satisfy Eq. (18), where f and g are two coefficients:

$$E_1\omega_1^f = E_2\omega_2^f \Rightarrow \frac{E_2}{E_1} = \left(\frac{\omega_1}{\omega_2}\right)^f = g \text{ or } \frac{\omega_1}{\omega_2} = \left(\frac{E_2}{E_1}\right)^{1/f} = g^{1/f} \quad (18)$$

Using Eq. (18) in Eqs. (3) and (4), the expressions of ε and φ are:

$$\begin{cases} \varepsilon = \frac{\sigma}{\beta E_1} (\omega_1^4 + 3\omega_1^2\omega_2^2g + 4\omega_1\omega_2^3g) \\ \varphi = \frac{\sigma}{\beta E_1} (6\omega_1^2\omega_2g + 6\omega_1\omega_2^2g) \end{cases} \quad (19)$$

where

$$\beta = \omega_1^4 + 4\omega_1^3\omega_2g + 6\omega_1^2\omega_2^2g + 4\omega_1\omega_2^3g + \omega_2^4g^2 \quad (20)$$

The J -integral and stress intensity factor K can be then derived, shown in Eqs. (21) and (22), respectively:

$$J = \frac{\sigma^2}{2\beta E_1} (\omega_1^4\omega_2g + \omega_1\omega_2^4g^2) \quad (21)$$

$$K = \sigma \cosh(\pi\alpha) \sqrt{\frac{\omega_1^4\omega_2g + \omega_1\omega_2^4g^2}{\beta(1+1/g)}} \quad (22)$$

A notable phenomenon is that the expressions of K in Eqs. (2) and (22) are not

Using Eqs. (11) and (13) in Eq. (12), the stress intensity factor K of the case in Fig. 2 can be obtained:

dependent on the half-length of the ligament or bi-material interface a . This indicates that Eqs. (2) and (22) could be also used to obtain the stress intensity factors of the cases in Fig. 1 (b) and Fig. 2 (b), respectively. For identical materials, this has been confirmed in previous studies [22, 26, 27].

Additionally, in other particular cases, several further simplified expressions of K can be obtained based on Eq. (22). If the value of g is set to ω_1/ω_2 , $(\omega_1/\omega_2)^2$, or $(\omega_1/\omega_2)^3$ (i.e., $f = 1, 2$, or 3), the corresponding expressions of K are:

$$K_{f=1} = \sigma \sqrt{\omega_1} \cosh(\pi\alpha) \times \sqrt{\frac{\omega_1}{\omega_1 + \omega_2}} \sqrt{\frac{\omega_1^2 + \omega_2^2}{5\omega_1^2 + 6\omega_1\omega_2 + 5\omega_2^2}} \quad (23)$$

$$K_{f=2} = \sigma \sqrt{\omega_1} \cosh(\pi\alpha) \times \sqrt{\frac{\omega_1^2}{\omega_1^2 + \omega_2^2}} \sqrt{\frac{\omega_1}{4\omega_1 + 4\omega_2}} \quad (24)$$

$$K_{f=3} = \sigma \sqrt{\omega_1} \cosh(\pi\alpha) \times \sqrt{\frac{\omega_1^3}{\omega_1^3 + \omega_2^3}} \sqrt{\frac{2\omega_1^2}{5\omega_1^2 + 6\omega_1\omega_2 + 5\omega_2^2}} \quad (25)$$

If the value of f approaches $+\infty$ (i.e., $\omega_1/\omega_2 = 1$), the expression of K is:

$$K_{\omega_1=\omega_2} = \sigma \sqrt{\omega_1} \cosh(\pi\alpha) \times \sqrt{\frac{E_2^2}{E_1^2 + 14E_1E_2 + E_2^2}} \quad (26)$$

4 NUMERICAL ANALYSIS

The above testing method for interface shear fracture can be utilized to investigate the shear behavior of the interface of different concrete materials. In this section, a numerical

analysis based on the proposed method is carried out to confirm its suitability for shear fracture tests. We focus on the interface between a UHTCC and plain concrete. The material properties (Table 1) for the numerical analysis were obtained from the experiment performed in this study.

Table 1 Material properties

Property	UHTCC	Plain concrete
Elastic modulus (GPa)	17.0	25.4
Poisson's ratio	0.19	0.20
Compressive strength (MPa)	44.0	29.5
Tensile strength (MPa)	3.0	2.5
Fracture energy* (N/m)	5371 [36]	150 [37]

* The fracture energies are obtained from previous studies.

Based on these two materials, four types of models, shown in Fig. 4 (a) and (b), are developed using a commercial finite-element analysis software (ABAQUS 2014). The identifications (IDs) and dimensions of the models are presented in Table 2. In the model ID, “A” represents the length of the interface, and “U” represents the width of the UHTCC edge. These models correspond to the particular cases discussed in Section 3. The

ratio of the concrete’s modulus (E_1) to the UHTCC’s modulus (E_2) is approximately 3/2. Therefore, for the cases $\omega_1 = \omega_2$, $E_1\omega_1 = E_2\omega_2$, $E_1\omega_1^2 = E_2\omega_2^2$, and $E_1\omega_1^3 = E_2\omega_2^3$, the ratios of ω_1 to ω_2 are set to 100:100, 100:115, 100:125, and 100:150 (Fig. 4 (a)), respectively. Additionally, the unnotched concrete/UHTCC specimens (shown in Fig. 4 (b)) are modelled.

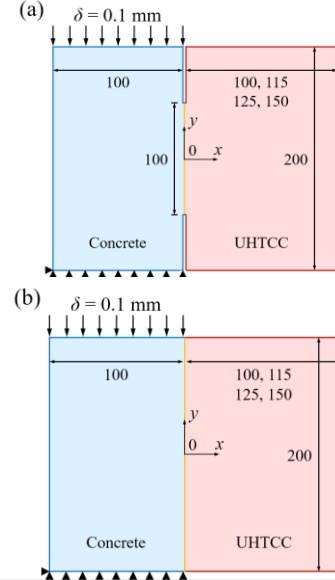


Fig. 4 (a) Notched concrete/UHTCC, and (b) unnotched concrete/UHTCC models for the finite-element analysis

Table 2 Model IDs and dimensions

Model ID	Material 1	Material 2	2a (mm)	ω_1 (mm)	ω_2 (mm)	2h (mm)
A100U100		UHTCC			100	
A100U115		UHTCC			115	
A100U125	Plain concrete	UHTCC	100	100	125	200
A100U150		UHTCC			150	
A200U100		UHTCC			100	
A200U115		UHTCC			115	
A200U125	Plain concrete	UHTCC	200	100	125	200
A200U150		UHTCC			150	

In the finite-element analysis, two-dimensional models were developed, as the double-edge notched compression test for bi-materials shown in Fig. 2 is performed under a plane stress. A tie constraint was employed to make the translational and rotational motions equal for the pair of surfaces. It is worth noting that the numerical analysis is focused on the stress distributions before the crack formation to confirm the result that the interface crack is

caused by a shear fracture. A displacement loading (0.1 mm) was applied on each model.

The results of the finite-element analysis are presented in Fig. 5 and Fig. 6. For the notched concrete/UHTCC models in Fig. 5, notable shear stress (τ_{xy}) concentrations can be observed at the notch tips (Fig. 5 (a)); in addition, the x -directional normal stress (σ_x) is close to zero (Fig. 5 (b)). The stress distributions of the unnotched concrete/UHTCC models are presented in Fig.

6. Similar to the notched models, shear stress (τ_{xy}) concentrations are observed at the ends of the interfaces (Fig. 6 (a)). These phenomena

indicate that the double-edge notched and unnotched specimen are suitable for the interface shear fracture tests.

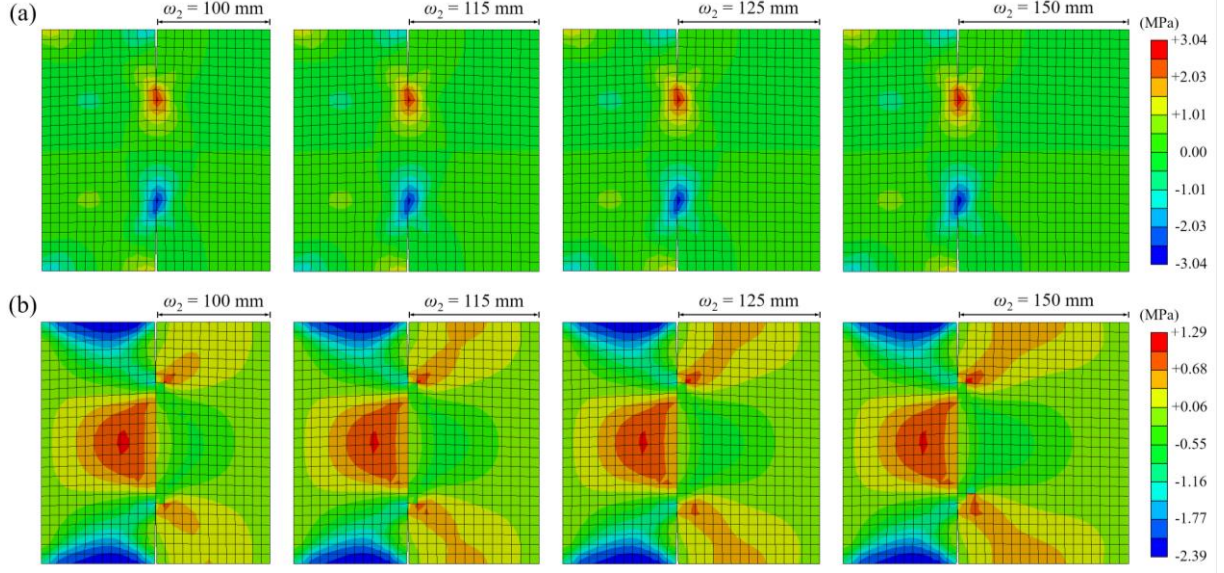


Fig. 5 Stress distributions of the notched concrete/UHTCC models (A100U100, A100U115, A100U125, and A100U150): (a) shear stress τ_{xy} and (b) x -directional normal stress σ_x distributions

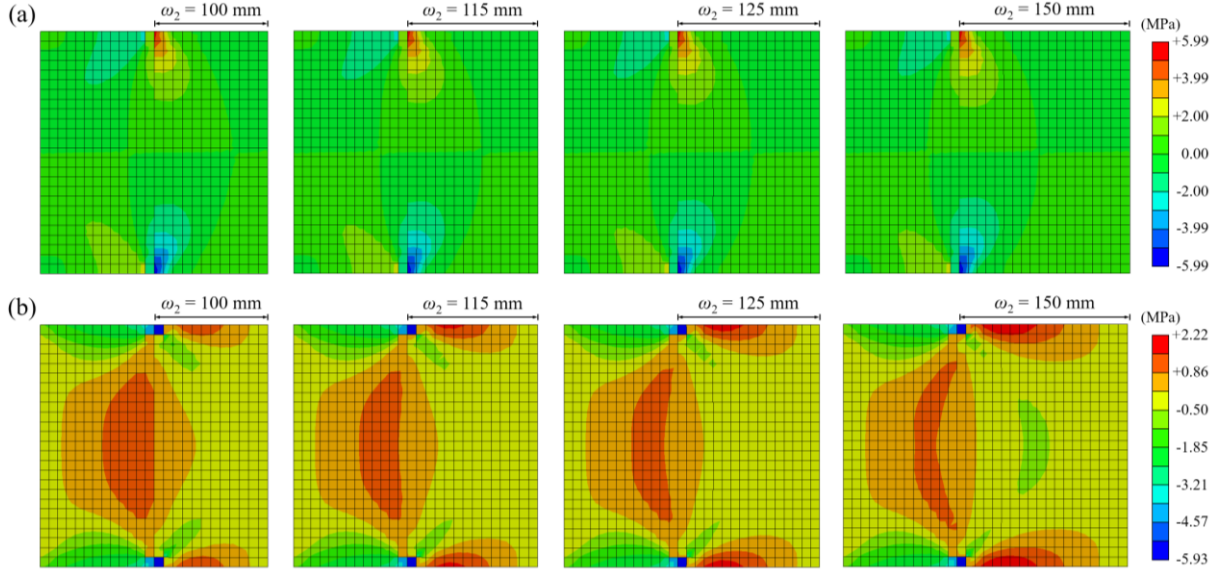


Fig. 6 Stress distributions of the unnotched concrete/UHTCC models (A200U100, A200U115, A200U125, and A200U150): (a) shear stress τ_{xy} and (b) x -directional normal stress σ_x distributions

5 EXPERIMENTAL VERIFICATION

In this section, an experimental investigation is carried out to validate the applicability of the proposed method for the interface shear fracture tests. We focus on the UHTCC/concrete interfaces. According to the results of the numerical study, the influence of the width of the right edge (ω_2) on the stress distributions is very limited for the double-

edge specimens. Therefore, only one case (i.e., $E_1\omega_1 = E_2\omega_2$) from Sections 3 and 4 is experimentally investigated in this section. Additionally, using the finite-element analysis, we showed that both notched and unnotched specimens in Fig. 2 are suitable for the interface shear fracture tests. In this test, first, the unnotched specimen is selected, as the specimen without notch along the interface is

more convenient to prepare compared with the notched specimen. The specimens with notches could be experimentally investigated in future studies.

The material properties of the UHTCC and plain concrete (cured for 28 days) were measured (presented in Table 1) before the experiment; the obtained parameters were used in the above numerical study. According to the measured moduli of the UHTCC and concrete in Table 1, the double-edge unnotched specimens were prepared for the case of $E_1\omega_1 = E_2\omega_2$ (shown in Table 2). The thicknesses of all of the specimens were 100 mm.

The setup of the interface shear fracture test is shown in Fig. 7. The compressive load is applied on the 100-mm-wide edge. According to the previous studies [22, 23, 24], a uniform stress distribution is important for the double-edge compression test. Therefore, two steel blocks with dimensions of $150 \times 100 \times 100$ mm³ are used; a sheet of polytetrafluoroethylene (PTFE) is added between the specimen and steel blocks to eliminate the friction. In this study, a 1000-kN INSTRON testing system was used. The displacement-control load was applied with constant rates of 0.24 mm/min before the load reached 120 kN and 0.12 mm/min until the load decreased to 80% of the peak load. A pair of linear variable differential transformers (LVDTs) with a gauge length of 150 mm were attached at both sides of the interface to record the shortening of the materials. The crack tip opening displacement (CTOD) at the lower end of the interface and crack tip slipping displacement (CTSD) at the upper end of the interface were measured using a pair of extensometers. Additionally, the total

displacements between the machine platens and applied load were recorded during the test.

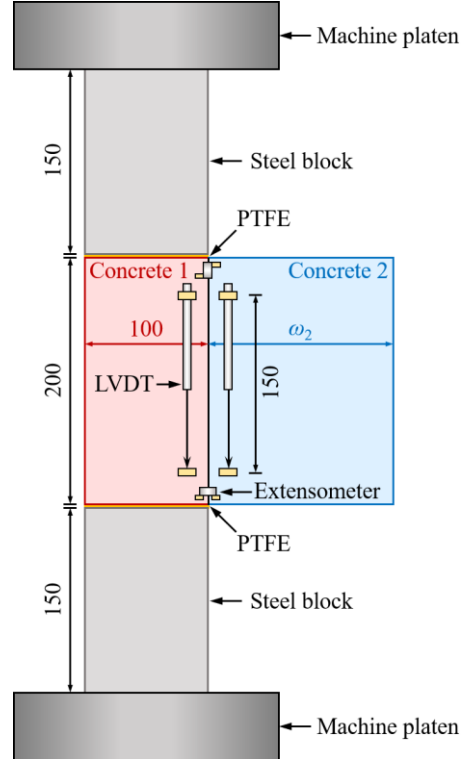


Fig. 7 Test setup

During the shear test, the interface fractures occurred and cracks were initiated from the upper or lower ends of the interfaces of all of the UHTCC/concrete specimens. The specimen IDs are presented in Table 3; four typical failure modes are selected and presented in Fig. 8. The failure modes of the UHTCC/concrete specimens are shown in Fig. 8 (a) and (b). Interface fractures are observed for all of the specimens in Fig. 8; in addition, compressive-load-induced cracks can be observed on the left edges of the specimens A200U150-1 and A200U150-2.

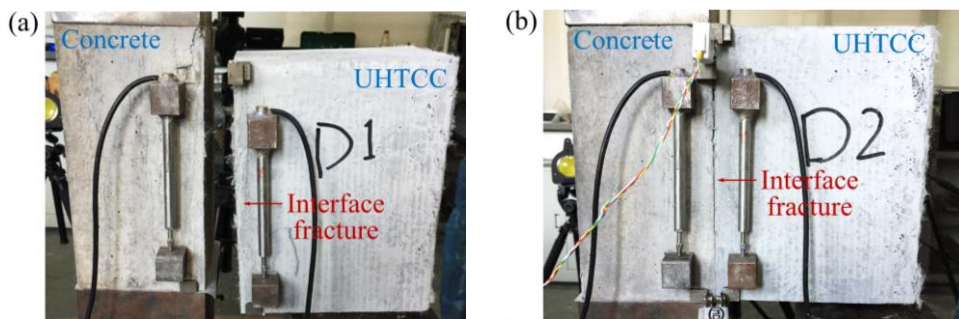


Fig. 8 Typical failure modes of the UHTCC/concrete specimens: (a) A200U150-1 and (b) A200U150-2

Table 3 Specimen IDs and critical parameters

Specimen ID	P_c (kN)	P_{\max} (kN)	P_c/P_{\max}	σ_c (MPa)	K_c (MPa·m ^{1/2})
A200U150-1	224	309	0.72	22.4	1.61
A200U150-2	270	323	0.84	27.0	1.94
A200U150-3	310	334	0.93	31.0	2.22
A200U150-4	195	320	0.61	19.5	1.40
A200U150-5	228	316	0.72	22.8	1.64
A200U150-6	200	289	0.69	20.0	1.44
Average	238	301	0.75	23.8	1.71

From the measured displacements, a few typical results are selected and shown in Fig. 9. For the specimen in Fig. 9, the displacements measured by the LVDTs and extensometers, as well as the displacement between the platens, are presented. It should be noted that the displacement between the platens includes the deformation of the PTFE layers; therefore, a nonlinear relation appears in the beginning of the loading, as shown in Figure 5 (a) in [23]. The displacement of each specimen in the first panel in Fig. 9 is corrected by subtracting the PTFE deformation from the total value. In Fig. 9, pronounced discontinuity points are observed at approximately 270 kN and 200 kN, respectively. After a small release, the load increases again. Similar phenomena were observed in the previous studies on shear fractures in identical concrete materials [22, 23, 24]. The discontinuity points can be also

observed in the records of the LVDTs (see the second panel of each group in Fig. 9). Additionally, a considerable displacement drop is observed from the record of LVDT2, related to the interface shear cracking, which released the stress of the material at the right side of the interface. The measured CTOD and CTSD are shown in the third panel; pronounced increases or discontinuity points can be observed in the curves, which are direct evidences of the interface cracking. According to these displacement records, it can be concluded that the discontinuity points are related to the interface shear cracking. Therefore, the loads corresponding to these points can be considered the critical loads for interface shear fracture. It should be noted that for identical concretes, this point is also defined as the critical point of shear fracture [22, 23, 24].

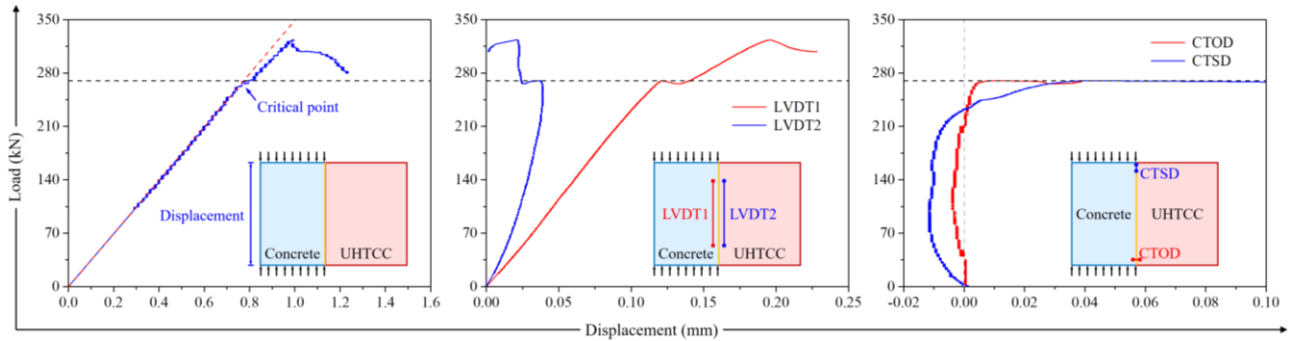


Fig. 9 Load–displacement curves of the UHTCC/concrete specimens: A200U150-2

For the other tested specimens, discontinuity points can be observed in some of their displacement records (they may not be observed in every record). The observed points can help determine the critical loads (P_c) of shear fracture for all of the specimens, which are presented in Table 3. Additionally, the

stress corresponding to the critical load (i.e., critical stress, σ_c) is obtained. It should be emphasized that the dimensions of the tested specimens obey the equation: $E_1\omega_1 = E_2\omega_2$. Therefore, Eq. (23) can be employed to calculate the critical stress intensity factors K_c of all of the specimens. Table 3 also presents

the peak load (P_{\max}) of each specimen. The average peak stresses of the specimens are 30.1 MPa, which is very similar to the measured compressive strength of the concrete (29.5 MPa). From the ratio of the critical load to the peak load (P_c/P_{\max}), it can be confirmed that the interface shear fracture occurred before the compressive failure of the concrete (approximately 75–80% of the peak load on average).

6 CONCLUSIONS

In this study, a novel testing method for interface shear fractures of plain concrete and fiber-reinforced cementitious composite was proposed. Analytical, numerical, and experimental investigations were carried out for the validation of this method. The double-edge notched and unnotched specimens were utilized in the proposed shear fracture testing method. The stress intensity factor K of the double-edge specimen with bi-materials was analytically obtained by the J -integral method. The detailed expressions of K were presented for four particular cases, including $\omega_1 = \omega_2$, $E_1\omega_1 = E_2\omega_2$, $E_1\omega_1^2 = E_2\omega_2^2$, and $E_1\omega_1^3 = E_2\omega_2^3$. Based on the UHTCC/concrete models, a numerical investigation of the proposed method was performed to confirm its suitability for shear fracture tests. The influence of the width of the UHTCC on the stress distributions was limited for the four particular cases. Finally, the double-edge UHTCC/concrete for one case were experimentally investigated. The interface fracture occurred and cracks were initiated from the upper or lower ends of the interface in each of the UHTCC/concrete specimens. In addition, the interface shear fracture occurred before the compressive failure of the concrete (on average, approximately 75–80% of the peak load). The discontinuity points of the load–displacement curves were considered the critical loads for interface shear fracture.

ACKNOWLEDGEMENTS

The authors would like to acknowledge the financial support from the National Natural Science Foundation of China under Grant Nos. 51622811 and 51678522. The authors also

thank Mr. Xiao-Hua Ji and Mr. Yu Peng at the College of Civil Engineering and Architecture of the Zhejiang University for their supports in the experiments.

REFERENCES

1. Li, V. C., Horii, H., Kabele, P., Kanda, T., & Lim, Y. M. (2000). Repair and retrofit with engineered cementitious composites. *Engineering Fracture Mechanics*, 65(2-3), 317-334.
2. Kim, Y. Y., Fischer, G., Lim, Y. M., & Li, V. C. (2004). Mechanical performance of sprayed engineered cementitious composite using wet-mix shotcreting process for repair applications. *ACI Materials Journal*, 101(1), 42-49.
3. Rokugo, K., Kanda, T., Yokota, H., & Sakata, N. (2009). Applications and recommendations of high performance fiber reinforced cement composites with multiple fine cracking (HPFRCC) in Japan. *Materials and structures*, 42(9), 1197.
4. Li, Q. H., Huang, B. T., & Xu, S. L. (2016). Development of assembled permanent formwork using ultra high toughness cementitious composites. *Advances in Structural Engineering*, 19(7), 1142-1152.
5. Huang, B. T., Li, Q. H., Xu, S. L., & Li, C. F. (2017). Development of reinforced ultra-high toughness cementitious composite permanent formwork: Experimental study and Digital Image Correlation analysis. *Composite Structures*, 180, 892-903.
6. Li, V. C., & Leung, C. K. (1992). Steady-state and multiple cracking of short random fiber composites. *Journal of Engineering Mechanics-ASCE*, 118(11), 2246-2264.
7. Li, V. C., Wang, S., & Wu, C. (2001). Tensile strain-hardening behavior of polyvinyl alcohol engineered cementitious composite (PVA-ECC). *ACI Materials Journal*, 98(6), 483-492.
8. Yu, K. Q., Yu, J. T., Dai, J. G., Lu, Z. D.,

- & Shah, S. P. (2018). Development of ultra-high performance engineered cementitious composites using polyethylene (PE) fibers. *Construction and Building Materials*, 158, 217-227.
9. Li, V. C., & Hashida, T. (1993). Engineering ductile fracture in brittle-matrix composites. *Journal of Materials Science Letters*, 12(12), 898-901.
 10. Yu, J., Yao, J., Lin, X., Li, H., Lam, J. Y., Leung, C. K., Sham I. M. L., & Shih, K. (2018). Tensile performance of sustainable Strain-Hardening Cementitious Composites with hybrid PVA and recycled PET fibers. *Cement and Concrete Research*, 107, 110-123.
 11. Li, H., Xu, S., & Leung, C. K. Y. (2009). Tensile and flexural properties of ultra high toughness cementitious composite. *Journal of Wuhan University of Technology-Mater. Sci. Ed.*, 24(4), 677-683.
 12. Huang, B. T., Li, Q. H., Xu, S. L., & Zhou, B. M. (2017). Frequency effect on the compressive fatigue behavior of ultrahigh toughness cementitious composites: experimental study and probabilistic analysis. *Journal of Structural Engineering-ASCE*, 143(8), 04017073.
 13. Huang, B. T., Li, Q. H., Xu, S. L., & Zhou, B. M. (2018). Tensile fatigue behavior of fiber-reinforced cementitious material with high ductility: Experimental study and novel P-S-N model. *Construction and Building Materials*, 178, 349-359.
 14. Suthiwarapirak, P., Matsumoto, T., & Kanda, T. (2004). Multiple cracking and fiber bridging characteristics of engineered cementitious composites under fatigue flexure. *Journal of Materials in Civil Engineering-ASCE*, 16(5), 433-443.
 15. Zhou, J., Pan, J., & Leung, C. K. (2014). Mechanical behavior of fiber-reinforced engineered cementitious composites in uniaxial compression. *Journal of Materials in Civil Engineering-ASCE*, 27(1), 04014111.
 16. Huang, B. T., Li, Q. H., Xu, S. L., Liu, W., & Wang, H. T. (2018). Fatigue deformation behavior and fiber failure mechanism of ultra-high toughness cementitious composites in compression. *Materials & Design*, 157, 457-468.
 17. Huang, B. T., Li, Q. H., and Xu, S. L. (2018). Fatigue deformation model of plain and fiber-reinforced concrete based on the Weibull function. *Journal of Structural Engineering-ASCE*, 145(1), 04018234.
 18. Leung, C. K. Y., & Cao, Q., Development of pseudo-ductile permanent formwork for durable concrete structures. *Materials and Structures*, 2010, 43(7), 993-1007.
 19. Huang, B. T. (2018). Fatigue performance of strain-hardening fiber-reinforced cementitious composite and its functionally-graded structures. Ph. D. thesis, Zhejiang University.
 20. Chen, Y., Yu, J., & Leung, C. K. (2018). Use of high strength Strain-Hardening Cementitious Composites for flexural repair of concrete structures with significant steel corrosion. *Construction and Building Materials*, 167, 325-337.
 21. Espeche, A. D., & León, J. (2011). Estimation of bond strength envelopes for old-to-new concrete interfaces based on a cylinder splitting test. *Construction and Building Materials*, 25(3), 1222-1235.
 22. Reinhardt, H. W., Ošbolt, J., Xu, S., & Dinku, A. (1997). Shear of structural concrete members and pure mode II testing. *Advanced Cement Based Materials*, 5(3-4), 75-85.
 23. Reinhardt, H. W., & Xu, S. (1998). Experimental determination of K_{IIC} of normal strength concrete. *Materials and Structures*, 31(5), 296-302.
 24. Reinhardt, H. W., & Xu, S. (2000). A practical testing approach to determine mode II fracture energy GIIF for concrete. *International Journal of Fracture*, 105(2), 107-125.

25. Tada, H., Paris, P.C, Irwin, G. (1985). *The stress analysis of cracks handbook*, St Louis, Paris Productions Incorporated and Del Research Corporate, 2nd ed.
26. Xu, S., Reinhardt, H. W., & Gappoev, M. (1996). Mode II fracture testing method for highly orthotropic materials like wood. *International Journal of Fracture*, 75(3), 185-214.
27. Gao, H. B. (2008). *Study on determination of Mode I and Mode II fracture parameters for concrete*. PhD thesis, Dalian University of Technology. (in Chinese)
28. Rice, J. R. (1968). A path independent integral and the approximate analysis of strain concentration by notches and cracks. *Journal of Applied Mechanics*, 35(2), 379-386.
29. Radaj, D., & Zhang, S. (1991). Stress intensity factors for spot welds between plates of unequal thickness. *Engineering Fracture Mechanics*, 39(2), 391-413.
30. Radaj, D., & Zhang, S. (1992). Stress intensity factors for spot welds between plates of dissimilar materials. *Engineering Fracture Mechanics*, 42(3), 407-426.
31. Hutchinson, J. W., & Suo, Z. (1991). Mixed mode cracking in layered materials. *Advances in Applied Mechanics*, 29, 63-191.
32. Shih, C. F. (1991). Cracks on bimaterial interfaces: elasticity and plasticity aspects. *Materials Science and Engineering: A*, 143(1-2), 77-90.
33. Toya, M. (1992). On mode I and mode II energy release rates of an interface crack. *International Journal of Fracture*, 56(4), 345-352.
34. Yahsi, O. S., & Gocmen, A. E. (1987). Contact problem for two perfectly bonded dissimilar infinite strips. *International Journal of Fracture*, 34(3), 161-177.
35. Keer, L. M., & Guo, Q. (1990). Stress analysis for symmetrically loaded bonded layers. *International Journal of Fracture*, 43(1), 69-81.
36. Li, H., & Xu, S. (2011). Determination of energy consumption in the fracture plane of Ultra High Toughness Cementitious Composite with direct tension test. *Engineering Fracture Mechanics*, 78(9), 1895-1905.
37. Wittmann, F. H., Rokugo, K., Brühwiler, E., Mihashi, H., & Simonin, P. (1988). Fracture energy and strain softening of concrete as determined by means of compact tension specimens. *Materials and Structures*, 21(1), 21-32.